Simulating the Behavior of a 230 GHz SIS Mixer Using Multi-Tone Spectral Domain Analysis

John D. Garrett, Boon Kok Tan, Faouzi Boussaha, Christine Chaumont, and Ghassan Yassin

***Abstract*—We present a new software package, called QMix, for simulating the behavior of Superconductor / Insulator / Superconductor (SIS) mixers. The software uses a harmonic balance procedure to calculate the AC voltage across the SIS junction and multi-tone spectral domain analysis (MTSDA) to calculate the quasiparticle tunneling currents. This approach has two major advantages over other simulation techniques: (1) it can include an arbitrary number of higher-order harmonics, and (2) it can simulate the effect of multiple strong non-harmonic frequencies. This allows the QMix software to simulate a wide range of SIS mixer operation, including the effects of harmonics in the local-oscillator signal and gain saturation with respect to RF signal power.**

In this paper, we compare the simulated results from QMix to the measured performance of a 230 GHz SIS device, both to validate the software and to investigate the experimental data. To begin, we simulated the conversion gain of the mixer and we found excellent agreement with the experimental results. We were also able to recreate the broken photon step effect by adding higher- and lower-order harmonics to the LO signal. We then simulated a range of incident RF signal powers in order to calculate the gain saturation point. This is an important metric for SIS mixers because we require linear gain for reliable measurements and calibration. In the simulated results, we found both gain compression and gain expansion, which is consistent with other studies. Overall, these examples demonstrate that QMix is a powerful software package that will allow researchers to simulate the performance of SIS mixers, investigate experimental results and optimize mixer operation. We have made all of the QMix software open-source and we invite others to contribute to the project.

***Index Terms*—Superconductor / Insulator / Superconductor (SIS) tunnel junctions, SIS mixers, superconducting detectors, multi-tone spectral domain analysis, simulation software**

I. Introduction

To study the performance of Superconductor / Insulator / Superconductor (SIS) mixers, we require a quantum mechanical description of the SIS mixing process. This was first provided by Tucker [1]–[3] who presented a perturbation approach to calculate the electrical properties of SIS junctions. With this technique, the junction's response to the local-oscillator signal is calculated (large-signal analysis), and then the junction is linearized around this operating point to calculate the conversion gain and noise temperature of the mixer (small-signal analysis). Tucker's SIS mixing theory successfully predicted quantum limited noise performance [4] and conversion efficiencies greater than unity [5]–[8], but it made two critical assumptions: (i) that the higher-order harmonics are short-circuited by the intrinsic capacitance of the SIS junction, and (ii) that the total power of the RF signals is small enough to not influence the operating point of the local-oscillator signal.

To address the first assumption, a spectral-domain approach was developed to analyze the higher-order harmonics of the local-oscillator (LO) signal [9], [10]. In brief, each harmonic modulates the quasiparticle energy eigenstates by a phase factor. We can convolve these phase factors in the frequency domain to calculate the total phase factor of the LO signal, which is then used to calculate the time-averaged tunneling current and thereby the large-signal operating point. Using this spectral-domain technique, researchers at CalTech developed SuperMix [11], [12], a computer-aided design package for analyzing SIS mixers. SuperMix still uses Tucker's perturbation approach, but the higher-order harmonics of the LO signal are included, which can cause lower conversion efficiencies if they are too powerful [9].

The second assumption was then addressed by extending the spectral-domain analysis of the LO signal to include multiple large-signal tones [13]–[15]. Unlike Tucker's perturbation approach, with multi-tone spectral domain analysis (MTSDA), the junction is no longer linearized around an operating point, which allows MTSDA to simulate more general SIS junction behavior, including sub-harmonic pumping [15], [16] and gain saturation as a function of RF signal power [14], [17]. MTSDA can also potentially be applied to other multi-tone applications, such as harmonic mixing [18] and SIS amplification [19]. In particular, gain saturation is an important metric for SIS mixers, both for calibration and measurements. For example, without linear gain, we cannot use the Y-factor technique to measure the noise temperature of the SIS device. More importantly, if the SIS device is used for astronomical observations, non-linear gain will lead to errors in the measured flux values. Therefore, we need to know the saturation point of the mixer to avoid these issues. We cannot simulate this value with Tucker's perturbation approach or with SuperMix, but we can with MTSDA.

In short, MTSDA is a very powerful simulation technique that can aid in the design, characterization and operation of SIS mixers. It has two main advantages over Tucker's perturbation technique: (1) it can simulate an arbitrary number of higher-order harmonics, and (2) it can include multiple strong non-harmonic frequencies. In this paper, we present a new software package based on the MTSDA technique. The software is called QMix, which stands for "Quasiparticle Mixing", and it is hosted online as an open-source project. We then compare the simulated results from the QMix software to experimental data measured from a 230 GHz SIS device.

J.D. Garrett, B.-K. Tan and G. Yassin are at the University of Oxford, Oxford, U.K. E-mail: john.garrett@physics.ox.ac.uk.

F. Boussaha and C. Chaumont are at GEPI, Observatoire de Paris–PSL, Paris, France.

Manuscript received June 15, 2019; revised August 29, 2019.

This was done both as a means to validate the software and to understand the behavior of the device. In the following, we review the MTSDA technique in Sec. II and describe the new QMix software in Sec. III. Next, the SIS device is described in Sec. IV and the simulated results are compared to the experimental data in Sec. V-A. Lastly, we present the simulated gain saturation of the SIS device with respect to RF signal power in Sec. V-B.

II. Multi-tone Spectral Domain Analysis

MTSDA has already been presented in [13]–[15], [20], so here we will only provide an overview of the technique. To begin, MTSDA assumes that the voltage applied to the SIS junction is a superposition of sinusoidal voltages:

$$V(t) = V_0 + \sum_{f=1}^{F} \sum_{p=1}^{P} |V_p^{(f)}| \cos\left(p\,\omega^{(f)} t + \phi_p^{(f)}\right) \quad (1)$$

where V_0 is the DC bias voltage, $\omega^{(f)}$ is the fundamental frequency of tone f, and $|V_p^{(f)}|$ and $\phi_p^{(f)}$ are the amplitude and phase of the AC voltage, respectively. In this equation, the indices f and p represent the tone and harmonic, respectively, and we include a maximum of F tones and P harmonics.

Assuming that one side of the SIS junction is grounded, this voltage will modulate the quasiparticle energy eigenstates on the ungrounded side by a phase factor:

$$f(t) = \exp\left\{-j\,\omega_{\mathrm{gap}} \int_{-\infty}^{t} \left[V(\tau) - V_0\right]\, \mathrm{d}\tau\right\} \quad (2a)$$

$$= \prod_{f=1}^{F} \prod_{p=1}^{P} \sum_{n=-\infty}^{\infty} A_p^{(f)}(n)\, e^{-jnp\omega^{(f)}t} \quad (2b)$$

where $j{=}\sqrt{-1}$, $\omega_{\mathrm{gap}}{=}eV_{\mathrm{gap}}/\hbar$ is the gap frequency, e is the electron charge, V_{gap} is the gap voltage, and $\hbar{=}h/2\pi$ is the reduced Planck constant. Eqn. 2a and Eqn. 2b are related through the Jacobi-Angers equality and so the complex coefficient $A_p^{(f)}(n)$ is given by:

$$A_p^{(f)}(n) = J_n\left(\alpha_p^{(f)}\right)\, e^{-jn\phi_p^{(f)}} \quad (3)$$

where J_n is the n^{th} order Bessel function of the first kind, and $\alpha_p^{(f)}$ is the junction drive level, defined as:

$$\alpha_p^{(f)} = \frac{e\,|V_p^{(f)}|}{\hbar\, p\,\omega^{(f)}}\,. \quad (4)$$

In order to calculate the tunneling current, we require the Fourier transform of Eqn. 2:

$$W(\omega') = \frac{1}{2\pi} \int_{-\infty}^{\infty} \prod_{f} \prod_{p} \sum_{n} A_p^{(f)}(n)\, e^{j\left(\omega' - np\omega^{(f)}\right)t}\, \mathrm{d}t\,. \quad (5)$$

This equation is very complex and difficult to solve; however, for a single tone f and harmonic p, it reduces to:

$$W_p^{(f)}(\omega') = \sum_{n=-\infty}^{\infty} A_p^{(f)}(n) \cdot \delta(\omega' - p\,\omega^{(f)})\,. \quad (6)$$

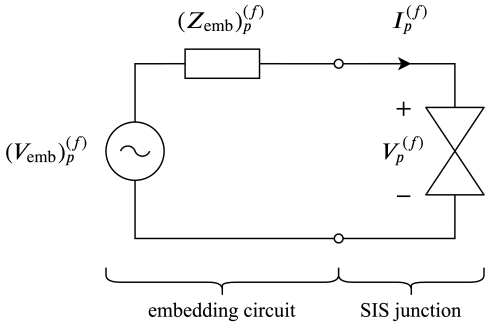

Figure 1. The embedding circuit for tone f and harmonic p. Here the SIS junction is shown on the right-hand side and the network within which the SIS junction is embedded is shown on the left. The AC voltage $V_p^{(f)}$ across the SIS junction is found through the harmonic balance procedure and the AC tunneling current $I_p^{(f)}$ is calculated using MTSDA. In this diagram, the intrinsic capacitance of the SIS junction is included within $(Z_{\mathrm{emb}})_p^{(f)}$.

Since the phase factor in the time-domain is the product of the individual tones and harmonics (Eqn. 2b), we can calculate the overall phase factor in the spectral-domain (Eqn. 5) by convolving the phase factors $W_p^{(f)}$ from each individual signal that is applied to the junction (see [13]–[15], [20]).

Finally, using Werthamer's relationship [21], the time-averaged tunneling current is calculated by:

$$\langle I(t)\rangle = \mathrm{Im} \iint_{-\infty}^{\infty} W(\omega') W^*(\omega'')\, e^{-j(\omega' - \omega'')t} \times I_{\mathrm{R}}(V_0 + \hbar\omega'/e)\, \mathrm{d}\omega' \mathrm{d}\omega'' \quad (7)$$

where W^* is the complex conjugate of W, and I_{R} is the response function of the SIS junction:

$$I_{\mathrm{R}}(V_0) = I_{\mathrm{kk}}(V_0) + jI_{\mathrm{dc}}^0(V_0)\,. \quad (8)$$

In Eqn. 8, the imaginary component is the DC current–voltage relationship (i.e., the DC I–V curve; $I_{\mathrm{dc}}^0(V_0)$) and the real component is found through the Kramers-Kronig transform:

$$I_{\mathrm{kk}}(V_0) = \frac{1}{\pi}\, \mathcal{P} \int_{-\infty}^{\infty} \frac{I_{\mathrm{dc}}^0(V') - V'/R_{\mathrm{n}}}{V' - V}\, \mathrm{d}V' \quad (9)$$

where $\mathcal{P}$ represents the Cauchy principal value integral, and R_{n} is the normal-state resistance of the SIS junction.

Using Eqns. 1–9, we can calculate the AC tunneling current $I_p^{(f)}$ at any tone f and harmonic p, which is generated by the set of all AC voltages, $V_p^{(f)}$. However, the exact value of each AC voltage component $V_p^{(f)}$ depends upon the network within which the SIS junction is embedded. Assuming that this embedding network is entirely linear, it can be reduced to a Thévenin equivalent circuit with a voltage V_{emb} and an impedance Z_{emb}, as shown in Fig. 1. Note that there is an individual Thévenin circuit for each unique signal that is applied to the junction.

The challenge is then to determine the set of all AC voltages, $V_p^{(f)}$, that satisfies:

$$(V_{\mathrm{emb}})_p^{(f)} - I_p^{(f)} \cdot (Z_{\mathrm{emb}})_p^{(f)} - V_p^{(f)} = 0 \quad (10)$$

for every tone f and harmonic p, simultaneously. Solving Eqn. 10 is difficult because $I_p^{(f)}$ is a highly non-linear function of the AC voltage and it also depends on the entire set of AC voltage components (i.e., $V_p^{(f)}$ for each f and p combination). The process of solving these equations simultaneously is generally known as harmonic balance.

For this paper, we used the Newton-Raphson method to solve Eqn. 10 and thereby calculate the steady-state AC voltage across the junction [10], [13]. Provided with an adequate initial guess, this technique has a quadratic rate of convergence and typically requires fewer than 5 iterations to find a solution (although, this depends on the embedding circuit, the properties of the DC I–V curve, and the number of signals applied to the junction). Practical information on implementing this harmonic balance procedure can be found in [10], [13], [20], along with a more detailed description of MTSDA.

III. The QMix Software Package

Using the MTSDA technique and the harmonic balance procedure, we developed a new software package to simulate the performance of SIS mixers. The package is called QMix [22], short for "Quasiparticle Mixing", and it is written in the Python programming language. Python is a high-level interpreted language that is easily portable to different machines and operating systems. QMix uses the scientific Python libraries extensively, including NumPy [23], SciPy [24], Matplotlib [25] and Numba [26]. These packages are highly optimized, which allows QMix to run quickly and with fewer errors.

The entire QMix project is hosted on GitHub in a public repository[1] that is automatically archived after each new release[2]. It is also available for download through the Python Package Index[3] (PyPI) , which is the official package manager for Python. All of the code is open-source under a GNU General Public License, meaning that anyone can download, use, distribute or modify the source code. The project also has an extensive website[4] that describes how to install and utilize the software, and it contains several examples that demonstrate how to setup QMix simulations.

Currently, QMix can simulate 4 non-harmonic frequencies and an arbitrary number of harmonics. This is enough for QMix to simulate double-sideband (DSB) SIS mixers, and we hope to add more frequencies in the near future. We also hope to add the ability to simulate multi-junction SIS devices and to calculate the noise properties of SIS mixers. Through the GitHub repository, other researchers are free to contribute to the project and add new features as needed.

IV. The 230 GHz SIS Device

The 230 GHz SIS device has already been presented in [20], [27], so here we will only briefly summarize the design. The planar circuit of this SIS device is shown in Fig. 2. It is a single-ended device, meaning that the LO and RF signals arrive together via the same optical path. The device uses a unilateral finline to couple these signals from the waveguide to the planar circuit [28], allowing the chip to sit in the E-plane of the waveguide. As shown on the right-hand side of Fig. 2, the width of the finline first tapers down to a slotline structure, before it transitions to a microstrip using two radial stubs. The SIS junction is a circular 1.5 μm^2 Nb/Al/AlO$_x$/Nb junction, with a normal-state resistance of $\sim$14 Ω and an estimated capacitance of 120 fF. The junction is situated between two tuning structures to cancel the effects of its parasitic capacitance. Finally, there are RF chokes to prevent the high-frequency signals from leaking into the IF circuitry and pads for the bond wires.

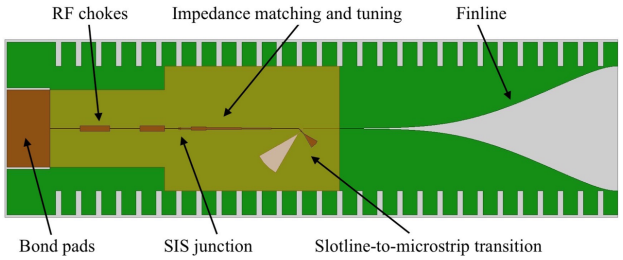

Figure 2. The planar circuit of the 230 GHz SIS device. The RF and LO signals arrive from the right-hand side and couple to the planar circuit through the finline. The microstrip has tuning structures to match to the impedance of the SIS junction and to cancel out the junction's capacitance.

All of the SIS devices were fabricated at l'Observatoire de Paris. The wiring and ground layers are 400 nm and 250 nm thick niobium, respectively, and the dielectric layer is made from 490 nm thick silicon monoxide. The devices were fabricated on a 300 μm thick quartz wafer, which was thinned afterwards to 100 μm.

V. Comparison Between Experimental and Simulated Results

For QMix to simulate the performance and recreate the experimental results from the 230 GHz SIS device, the software requires: (a) the response function of the SIS junction, and (b) the embedding circuit for each signal that is applied to the mixer. Both of these properties can be recovered from the experimental data; however, the embedding impedance can also be simulated using electromagnetic simulation software.

In Fig. 3, we plot the embedding impedance of the SIS device at different LO frequencies. For the experimental data, we recovered the embedding impedances from the pumped I–V curves, following [29], [30]. For the "HFSS" results, we simulated the reflection coefficient seen by the junction ($S_{J,J}$) using full-wave electromagnetic simulation software (ANSYS High Frequency Structural Simulator; HFSS) and then we calculated the embedding impedance using:

$$Z_{\mathrm{emb}} = Z_{\mathrm{j}} \left(\frac{1 + S_{J,J}}{1 - S_{J,J}} \right) \tag{11}$$

where Z_{j} is the port impedance of the SIS junction in the simulation model. We used Z_{j}=9.5 Ω$\sim^2/_3 \cdot R_{\mathrm{n}}$; although, the chosen port impedance will not affect the simulated Z_{emb}

[1]Online: https://github.com/garrettj403/QMix
[2]Online: https://zenodo.org/record/2640907
[3]Online: https://pypi.org/project/QMix/
[4]Online: https://garrettj403.github.io/QMix/

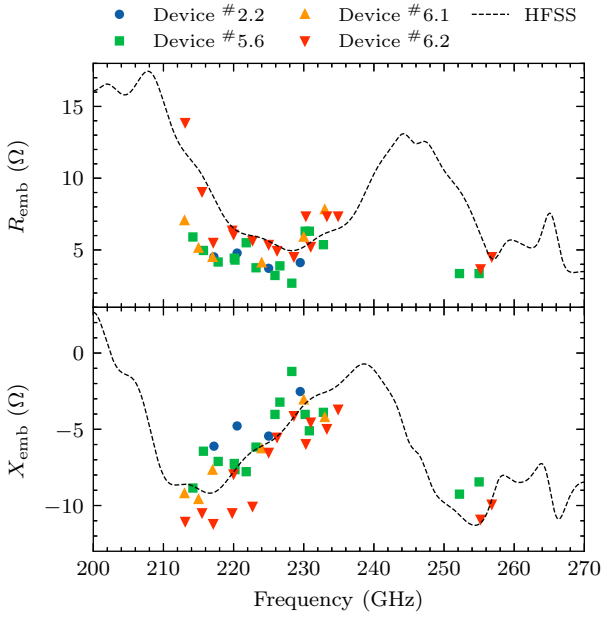

Figure 3. The embedding impedance of the 230 GHz SIS device: $Z_{\rm emb}{=}R_{\rm emb}{+}jX_{\rm emb}$. The impedance calculated by HFSS is shown by the black dashed lines (smoothed by a Gaussian filter) and the impedances recovered from the experimental results are shown by the colored points. For the experimental data, we analyzed the pumped I–V curves from 4 different devices. (The numbers in the legend correspond to the serial numbers of these devices.) The RF range of this device extends from 140 GHz to 270 GHz, but we only tested them from 213 GHz to 257 GHz due to the limited tuning range of our LO. There are no experimental data points from 236 GHz to 255 GHz because the broken photon step effect (discussed in Sec. V) prevented us from recovering these embedding impedances.

value. In the HFSS simulation, we also included the complex surface impedance of the niobium superconductors, which we calculated using Mattis-Bardeen theory [31].

As seen in Fig. 3, the agreement between the experimental and simulated embedding impedances is very good. The scatter in the experimental data points could be caused by several factors, such as minor differences in the dimensions of the device or variable junction sizes; however, even with the scatter, the simulated results from HFSS managed to accurately reproduce the general profile of the experimental data. For the comparisons in this paper, we will recreate the measured performance of device #6.2 because the experimental embedding impedances from this device provided the closest fit to the simulated results from HFSS.

Using the QMix software, we then created a 4-tone simulation with unique frequencies for the local-oscillator (LO), the upper sideband (USB), the lower sideband (LSB) and the intermediate frequency (IF) signals. The IF frequency was set to 5 GHz because the experimental results were measured with a $4{-}6$ GHz bandpass filter. For each frequency, we also included two higher-order harmonics. Since the junction is relatively large, we do not expect any higher-order harmonics past this point to influence the simulated gain value. The response function was then generated from the experimental DC I–V curve, and the embedding impedance for each unique signal was simulated with HFSS.

A. Conversion Gain

The simulated conversion gain from QMix is plotted in Fig. 4 for 9 different LO frequencies. In most instances, there is very good agreement between the experimental and simulated results. We suspect that some of the discrepancy in Fig. 4 is due to small errors in the simulated embedding impedances from HFSS. For example, at 230.3 GHz, the maximum simulated conversion gain is 1.19 using the embedding impedance from HFSS, but this decreases to 1.02 if we use the embedding impedance recovered from the experimental data, which is closer to the measured value of 0.89. For this paper, we used the embedding impedances from HFSS to demonstrate how the QMix software can be used to simulate new, untested devices; although, QMix can also be used to analyze the experimental results once the devices have been tested. Another potential source for errors in Fig. 4 is that the simulation used an IF frequency of 5 GHz (i.e., a single frequency), while the experimental data was measured from 4–6 GHz using a bandpass filter.

In general, the QMix software was able to closely recreate the experimental results from the SIS device; however, from 236 GHz to 255 GHz, there are large dips in the measured gain values, which are not seen in the simulated results. This is a phenomena commonly known as the broken photon step effect, and it is characterized by a large notch in the pumped I–V curve at $V_0{=}V_{\rm gap}{-}hf_{\rm LO}/2e$ (where $f_{\rm LO}$ is the LO frequency) and a corresponding decrease in output power at the same voltage. The broken photon step effect significantly degrades the mixer's performance as it occurs at the bias voltage where the best performance is normally found. It also reduces the saturation point of the mixer by $\sim$50% because the effective width of the photon step is divided in two[5].

The broken photon step effect was previously investigated by Ermakov *et al.* [33]. They found that the appearance of the effect does not depend on the magnetic field, implying that the broken steps are not related to the Josephson effect. In contrast, they did find that the effect scales with temperature (i.e., as the temperature of the SIS junction increases, the gap voltage decreases, and with it, the position of the broken photon step), suggesting that the effect is largely related to the quasiparticle tunneling current. This lead Ermakov *et al.* to propose that the broken photon steps could be caused by spurious harmonics from the LO source at either $1/2{\cdot}f_{\rm LO}$ or $3/2{\cdot}f_{\rm LO}$.

For our device, the expected power transmission between the input waveguide and the SIS tunnel junction is approximately -125 dB at $1/2{\cdot}f_{\rm LO}$ and -5 dB at $3/2{\cdot}f_{\rm LO}$. Therefore, it is unlikely that the sub-harmonic signal at $1/2{\cdot}f_{\rm LO}$ is able to propagate from the LO source to the SIS junction, and it is much more probable that the broken photon steps are caused by the spurious tone at $3/2{\cdot}f_{\rm LO}$. In order to investigate this hypothesis using our QMix model, we added lower- and higher-order harmonics to the LO signal at $1/2{\cdot}f_{\rm LO}$ and $3/2{\cdot}f_{\rm LO}$. The power of the primary LO signal (at $f_{\rm LO}$) was then set to 38.9 nW, and the powers of the $1/2{\cdot}f_{\rm LO}$ and

[5]Following the description from Kerr [32], the saturation point of the mixer is related to the magnitude of the IF output voltage relative to the width of the photon step. Therefore, if the width of the step is divided in two, the saturation point should also drop by approximately 50%.

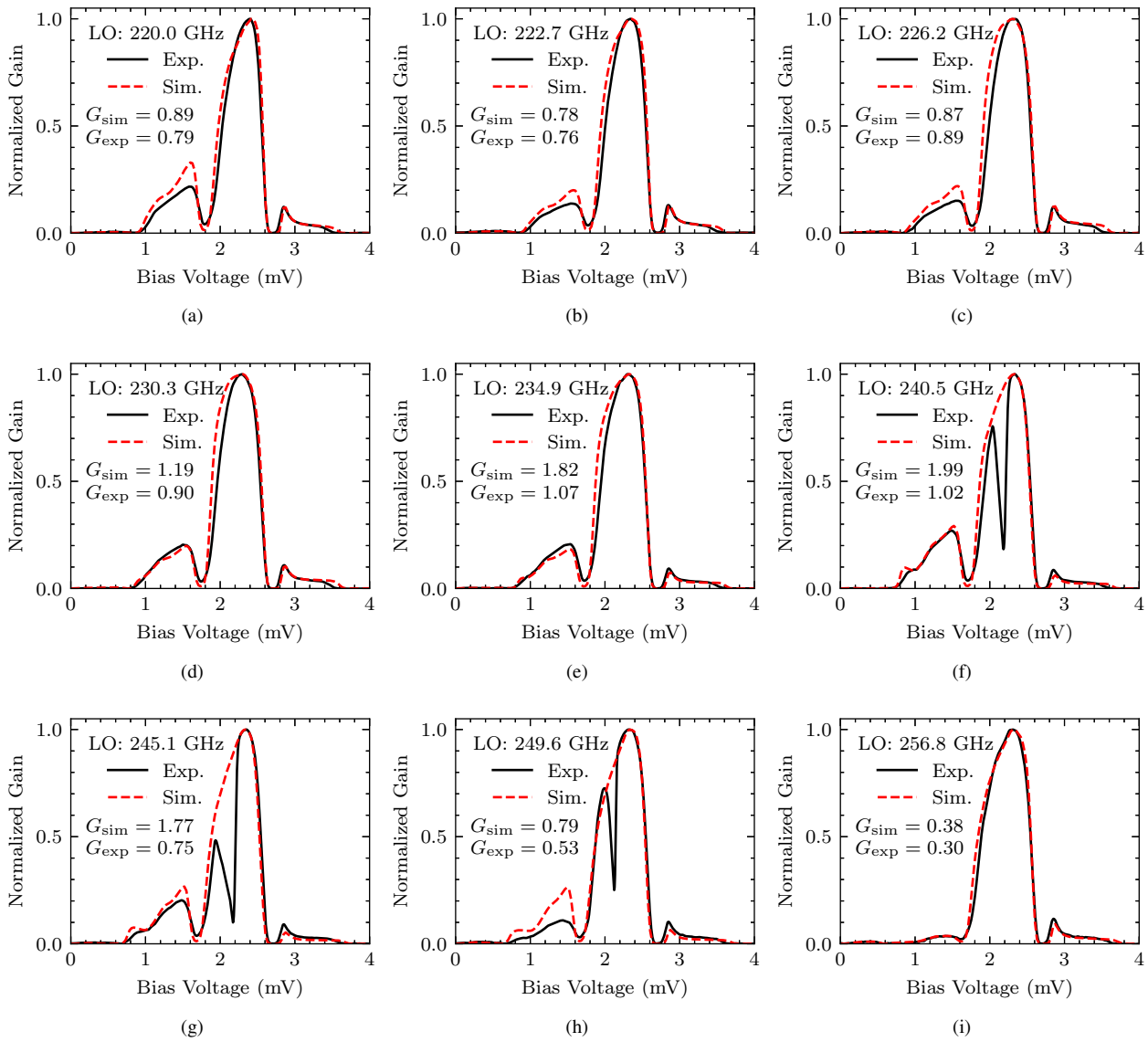

Figure 4. The measured conversion gain of device #6.2 compared to the simulated results from QMix. In each plot, the gain values are normalized to their maximum value. The maximum values for the experimental and simulated results are listed in the legends (G_{exp} and G_{sim}, respectively). The LO frequency is also listed above each legend. This simulation included 4 tones (LO, USB, LSB and IF) and 3 harmonics for each tone. The embedding impedances for each signal were simulated using HFSS. The IF frequency was set to 5 GHz because the experimental results were integrated from 4–6 GHz.

$^3/_2 \cdot f_{LO}$ harmonics were set to 0 nW and 6.3 nW, respectively. (These powers were recovered from the experimental data by matching the pumped I–V curves.) The updated results from QMix are shown in Fig. 5. Compared to the previous results in Fig. 4f, there is much better agreement between the simulated and measured results, both in terms of shape and absolute value, suggesting that the spurious tone at $^3/_2 \cdot f_{LO}$ is indeed the cause of the broken photon step effect.

It is important to note that we included the sub-harmonic signal in the simulation even though the power was set to zero because we suspected that the embedding impedance at this frequency could influence the severity of the broken photon steps. As shown in Fig. 6, the embedding impedance becomes extremely inductive in a certain frequency range around $^1/_2 \cdot f_{LO}$. This range coincides exactly with the LO frequency range where we observed the broken photon steps in Fig. 4 (from 236–255 GHz). This implies that the embedding impedance around this frequency range is very influential to the mixer's performance, despite having no power applied to the junction at $^1/_2 \cdot f_{LO}$.

In order to validate this assumption, we repeated the same simulation from Fig. 5, except that we set both the embedding impedance and the embedding voltage to zero for the sub-harmonic signal (instead of only setting the voltage to zero, as we did previously). The new simulation is shown in Fig. 7. As expected, the broken photon step effect almost completely disappears. This demonstrates that the embedding impedance of the sub-harmonic is important and that it should be considered when designing SIS mixers. Inductive embedding impedances at $^1/_2 \cdot f_{LO}$ should either be avoided, or when this is not possible, the LO signal should be filtered to reduce the power of the spurious harmonics.

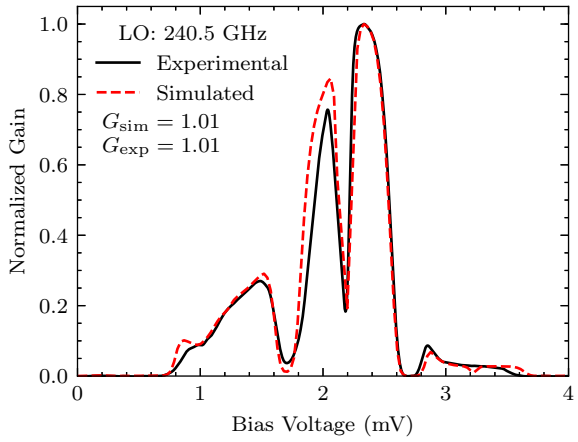

Figure 5. Simulating the broken photon step at 240.5 GHz by adding a spurious signal at $^3/_2{\cdot}f_{\rm LO}$. The power of the primary LO signal at $f_{\rm LO}$ was set to 38.9 nW, and the power of the spurious signal at $^3/_2{\cdot}f_{\rm LO}$ was set to 6.3 nW. The sub-harmonic at $^1/_2{\cdot}f_{\rm LO}$ was also included in the simulation, but the embedding voltage was set to zero (i.e., no power was applied at this frequency). All of the embedding impedances were derived from the HFSS simulations.

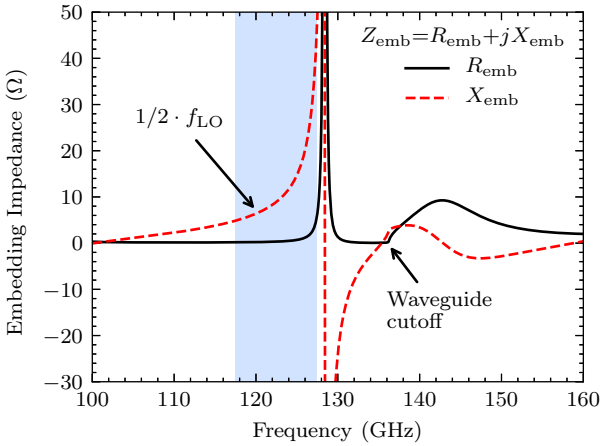

Figure 6. The simulated embedding impedance for the sub-harmonic LO signal at $^1/_2{\cdot}f_{\rm LO}$. The real component is shown in black ($R_{\rm emb}$) and the imaginary in red ($X_{\rm emb}$). The broken photon step effect occurs with this device between 236 GHz and 255 GHz. For the $^1/_2{\cdot}f_{\rm LO}$ signal, this corresponds to 118−127.5 GHz (depicted above by the pale blue region). The embedding impedance is very inductive over this range. Note that this SIS device is mounted in a 1.1 mm × 0.55 mm rectangular waveguide, which has a cutoff frequency of 136 GHz. No signals should be able to propagate below this frequency; although, the input impedance of the waveguide will become very reactive, which could cause the resonant behavior seen above.

In future work, we would like to simulate the full harmonic content of the LO signal and investigate how the harmonics influence the mixer's performance. This work would involve measuring the spectrum of the LO signal (e.g., using a Fourier-transform spectrometer), simulating the LO spectrum using QMix, and then evaluating the change in conversion gain. This work, however, is beyond the scope of this initial paper.

B. Gain Saturation

In the previous sub-section, we used QMix's ability to simulate multiple higher-order harmonics in order to recreate the broken photon step effect. Another advantage of the QMix software is that it can simulate multiple strong non-harmonic frequencies, allowing us to study gain saturation as a function of RF signal power. As we explained in the introduction, this is an important metric for SIS mixers because linear conversion gain is required for reliable measurements and calibration. Currently, there are no available software packages that are able to simulate gain saturation and so we require a new package, such as QMix, to model these effects.

For this simulation, we set the frequency of the LO signal to 220 GHz and then we swept the RF signal power upwards from −130 dBm. In Fig. 8, the gain saturation of the SIS mixer is plotted at three different IF frequencies (5 GHz, 10 GHz and 15 GHz) and two different DC bias voltages (∼1.4 mV and ∼2.2 mV). The gain saturation was calculated by:

$$\text{Gain saturation} = \frac{G\left(P_{\rm rf}\right)}{G_{\rm small}} \tag{12}$$

where $G\left(P_{\rm rf}\right)$ is the simulated conversion gain at a given RF signal power, and $G_{\rm small}$ is the simulated gain when the RF signal power approaches zero, i.e.:

$$G_{\rm small} = \lim_{P_{\rm rf}\to 0} G\left(P_{\rm rf}\right) . \tag{13}$$

For the RF signal, we only included the USB signal to simulate the mixer's response to a strong emission line[6]. The power level where the gain compression reaches −1 dB (commonly known as the 1 dB compression point, P1dB) is also labeled in Fig. 8. This value is a common figure of merit for electronic mixers because it generally defines the maximum RF input power that the mixer can receive before there is significant gain saturation.

As we can see in Fig. 8, the 1 dB compression point increases from −55.7 dBm at 5 GHz to −45.2 dBm at 15 GHz.

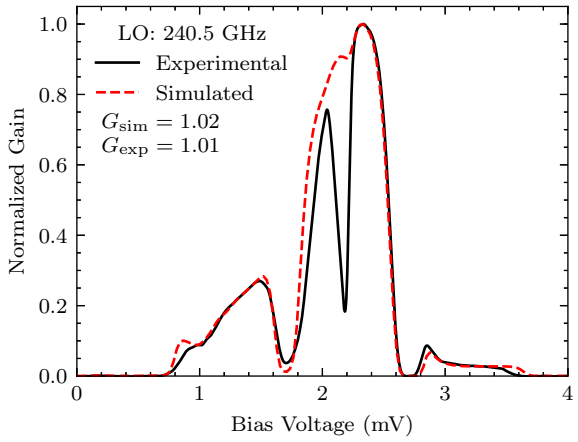

Figure 7. Simulating the broken photon step again at 240.5 GHz. This simulation used the same setup as Fig. 5, except that the embedding impedance of the sub-harmonic signal at $^1/_2{\cdot}f_{\rm LO}$ was set to zero. In this figure, the broken photon step is not as severe as it was in Fig. 5, implying that the highly-inductive embedding impedance at $^1/_2{\cdot}f_{\rm LO}$ aggravates the broken photon step effect.

[6]The gain saturation calculated by the MTSDA technique is only valid for continuous-wave (CW) input signals. For broadband noise (such as thermal radiation), the 1 dB compression point is typically several decibels lower due to the statistical nature of the noise [32].

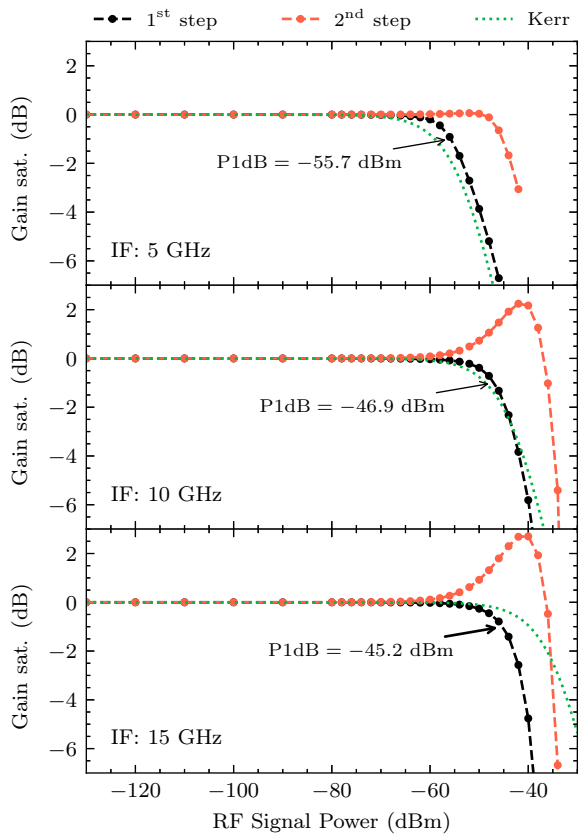

Figure 8. The simulated gain saturation at 220 GHz as a function of RF input signal power. The gain saturation is plotted for three different IF frequencies (5 GHz, 10 GHz and 15 GHz) and two different bias voltages: the middle of the first photon step (V_0∼2.2 mV) and the middle of the second step (V_0∼1.4 mV). The 1 dB compression point is labeled for the first photon step on each plot. We have also included the theoretical gain saturation from Eqn. 14 and Eqn. 15, following Kerr [32].

For 5 GHz and 10 GHz, we suspect that the change in the saturation point is mostly due to how the gain of this mixer decreases with rising IF frequency, thus allowing the mixer to handle higher input powers at higher IF frequencies. Following the analysis from Kerr [32], which describes how the gain of an SIS mixer saturates due to the down-converted IF voltage, the gain in Fig. 8 should saturate as:

$$G(P_{\rm rf}) = G_{\rm small}\left(1+\frac{P_{\rm rf}}{P_{\rm sat}}\right)^{-1} \tag{14}$$

where $P_{\rm sat}$ is the 3 dB saturation point:

$$P_{\rm sat} = C_{\rm sat}\frac{N^2\, f_{\rm LO}^2}{G_{\rm small}\, R_{\rm L}}\,, \tag{15}$$

$C_{\rm sat}$=1.7×10^{30} is an empirical constant that is approximately the same for all SIS devices, N is the number of SIS junctions in series (N=1 for this device), and $R_{\rm L}$ is the load resistance. The results with the IF frequency set to 5 GHz and 10 GHz generally agree with the analysis from Kerr [32] for the first photon step[7], suggesting that the gain at these IF frequencies saturates due to the IF output voltage and that the increase in the P1dB value from 5 GHz to 10 GHz is due to the decrease in small-signal gain. With the IF frequency set to 15 GHz, the mixer saturates at a lower value than what is predicted by Kerr [32]. This is likely because the small signal gain is so low that the mixer saturates due to the RF input signal power instead (and not due to the IF output voltage). Generally, this occurs when the RF signal power approaches the LO power ($P_{\rm LO}$= − 44.6 dBm in this case).

Interestingly, the first photon step in Fig. 8 always experiences gain compression, while the second step experiences both gain compression and expansion. These results are consistent with the work of Tong *et al.* [34], who explains that the difference between gain compression and gain expansion is related to the second derivative of the gain curve, $G''(V_0)$, shown previously in Fig. 4a. For example, if $G''(V_0)$ is negative, as the IF output voltage modulates the effective DC bias voltage, the time-averaged gain will decrease and lead to gain compression. Conversely, if $G''(V_0)$ is positive, the time-averaged gain will increase and lead to gain expansion. For the first photon step (at V_0∼2.2 mV), the mixer is biased at the maximum $G(V_0)$ value, which has a negative second derivative. Therefore, following the work of Tong *et al.* [34], we should expect gain compression and that is what we do indeed observe in Fig. 8. In contrast, the second photon step is biased at a location on the gain curve that has a slightly positive $G''(V_0)$ value (at V_0∼1.4 mV). This leads to the small amount of initial gain expansion that we see in Fig. 8, before it too experiences gain compression.

We hope to verify the results from Fig. 8 with experimental measurements from the 230 GHz SIS device. However, for this paper, we were limited by the availability of clean LO sources, i.e., LO sources with low phase noise and low higher-order harmonics, which would influence the saturation results.

VI. Conclusion

We have presented a new software package, called QMix, that was developed using multi-tone spectral domain analysis. This software can simulate a wide range of SIS junction behavior, and unlike other packages, it can simulate multiple strong tones and an arbitrary number of higher-order harmonics. In this paper, we used both of these abilities to investigate the experimental results from a 230 GHz SIS device. First, we simulated the conversion gain of the SIS mixer and found excellent agreement with the experimental results. The software was also able to recreate the broken photon step effect, which was seen in some of the experimental results, by adding spurious harmonics to the LO signal. Through these simulations, we discovered that the effect is likely caused by a spurious harmonic at $^3/_2\cdot f_{\rm LO}$, but the severity the effect is aggravated by an inductive embedding impedance at $^1/_2\cdot f_{\rm LO}$. Therefore, in future mixer designs, one should be careful to avoid inductive embedding impedances at $^1/_2\cdot f_{\rm LO}$ and filter out any unwanted harmonics from the LO source. Next, we simulated the gain saturation of the SIS mixer with respect to RF signal power. These simulations allowed us to estimate the RF saturation point of the mixer, below which point the

[7]Eqn. 14 and Eqn. 15 are only valid for gain curves that are even functions about the chosen bias voltage. This is approximately true for the first step in Fig. 4a, but it is not true for the second step.

mixer has linear gain. In the simulated results, we found both gain compression and gain expansion, which is consistent with previous studies. Based on the success of these simulations, we are confident that QMix will be a powerful tool for analyzing experimental data, designing new SIS devices and optimizing mixer operation. QMix is open-source and we invite anyone to use the software and contribute to the project.

REFERENCES

[1] J. Tucker, "Quantum limited detection in tunnel junction mixers," *IEEE J. Quantum Electron.*, vol. 15, no. 11, pp. 1234–1258, Nov. 1979, doi: 10.1109/JQE.1979.1069931.

[2] ——, "Predicted conversion gain in superconductor-insulator-superconductor quasiparticle mixers," *Appl. Phys. Lett.*, vol. 36, no. 6, pp. 477–479, Mar. 1980, doi:10.1063/1.91513.

[3] J. Tucker and M. Feldman, "Quantum detection at millimeter wavelengths," *Rev. Mod. Phys.*, vol. 57, no. 4, pp. 1055–1113, Oct. 1985, doi:10.1103/RevModPhys.57.1055.

[4] P. L. Richards, T. M. Shen, R. E. Harris, and F. L. Lloyd, "Quasiparticle heterodyne mixing in SIS tunnel junctions," *Appl. Phys. Lett.*, vol. 34, no. 5, pp. 345–347, Mar. 1979, doi:10.1063/1.90782.

[5] T. Shen, P. L. Richards, R. E. Harris, and F. L. Lloyd, "Conversion gain in mm-wave quasiparticle heterodyne mixers," *Appl. Phys. Lett.*, vol. 36, no. 9, pp. 777–779, May 1980, doi:10.1063/1.91654.

[6] S. Rudner, M. Feldman, E. Kollberg, and T. Claeson, "The antenna-coupled SIS quasiparticle array mixer," *IEEE Trans. Magn.*, vol. 17, no. 1, pp. 690–693, Jan. 1981, doi:10.1109/TMAG.1981.1061162.

[7] W. R. McGrath, P. L. Richards, A. D. Smith, H. van Kempen, R. A. Batchelor, D. E. Prober, and P. Santhanam, "Large gain, negative resistance, and oscillations in superconducting quasiparticle heterodyne mixers," *Appl. Phys. Lett.*, vol. 39, no. 8, pp. 655–658, Oct. 1981, doi:10.1063/1.92809.

[8] A. Kerr, S.-K. Pan, M. Feldman, and A. Davidson, "Infinite available gain in a 115 GHz SIS mixer," *Physica B+C*, vol. 108, no. 1-3, pp. 1369–1370, Aug. 1981, doi:10.1016/0378-4363(81)90983-9.

[9] S. Withington and E. Kollberg, "Spectral-domain analysis of harmonic effects in superconducting quasiparticle mixers," *IEEE Trans. Microw. Theory Techn.*, vol. 37, no. 1, pp. 231–238, Jan. 1989, doi:10.1109/22.20043.

[10] S. Withington and P. Kennedy, "Numerical procedure for simulating the large-signal quantum behaviour of superconducting tunnel-junction circuits," *IEE Proceedings G Circuits, Devices and Systems*, vol. 138, no. 1, pp. 70–76, Feb. 1991, doi:10.1049/ip-g-2.1991.0014.

[11] J. Ward, F. Rice, and G. Chattopadhyay, "SuperMix: A Flexible Software Library for High-Frequency Circuit Simulation, Including SIS Mixers and Superconducting Elements," in *Proc. 10th Int. Symp. Space THz Tech.*, Charlottesville, VA, Mar. 1999, pp. 269–281.

[12] F. Rice, J. Ward, and J. Zmuidzinas, "Fast Harmonic Balance of SIS Mixers with Multiple Junctions and Superconducting Circuits," in *Proc. 10th Int. Symp. Space THz Tech.*, Charlottesville, VA, Mar. 1999, pp. 282–297.

[13] P. Kittara, "The Development of a 700 GHz SIS Mixer with Nb Finline Devices: Nonlinear Mixer Theory, Design Techniques and Experimental Investigation," DPhil thesis, University of Cambridge, 2002.

[14] S. Withington, P. Kittara, and G. Yassin, "Multitone quantum simulations of saturating tunnel junction mixers," *J. Appl. Phys.*, vol. 93, no. 12, pp. 9812–9822, Jun. 2003, doi:10.1063/1.1576515.

[15] P. Kittara, S. Withington, and G. Yassin, "Theoretical and numerical analysis of very high harmonic superconducting tunnel junction mixers," *J. Appl. Phys.*, vol. 101, no. 2, p. 024508, Jan. 2007, doi:10.1063/1.2424407.

[16] P. K. Grimes, G. Yassin, P. Kittara, and S. Withington, "Analysis of subharmonic SIS mixers using SuperMix," in *Proc. 17th Int. Symp. Space THz Tech.*, Paris, France, May 2006, pp. 94–97.

[17] P. K. Grimes, S. Withington, G. Yassin, and P. Kittara, "Quantum multitone simulations of saturation in SIS mixers," in *Proc. SPIE Astronomical Telescopes and Instrumentation*, J. Zmuidzinas, W. S. Holland, and S. Withington, Eds., vol. 5498, Oct. 2004, pp. 158–167, doi:10.1117/12.549781.

[18] K. V. Kalashnikov, A. V. Khudchenko, A. B. Baryshev, and V. P. Koshelets, "Harmonic mixer based on superconductor-insulator-superconductor tunnel junction," *J. Commun. Techn. Electron.*, vol. 56, no. 6, pp. 699–707, Jun. 2011, doi:10.1134/S106422691106009X.

[19] T. Kojima, Y. Uzawa, and W. Shan, "Microwave amplification based on quasiparticle SIS up and down frequency converters," *AIP Adv.*, vol. 8, no. 2, p. 025206, Feb. 2018, doi:10.1063/1.5013268.

[20] J. D. Garrett, "A 230 GHz Focal Plane Array Using a Wide IF Bandwidth SIS Receiver," DPhil thesis, University of Oxford, 2018.

[21] N. R. Werthamer, "Nonlinear Self-Coupling of Josephson Radiation in Superconducting Tunnel Junctions," *Phys. Rev.*, vol. 147, no. 1, pp. 255–263, Jul. 1966, doi:10.1103/PhysRev.147.255.

[22] J. D. Garrett and G. Yassin, "QMix: A Python package for simulating the quasiparticle tunneling currents in SIS junctions," *J. Open Source Softw.*, vol. 4, no. 35, p. 1231, Mar. 2019, doi:10.21105/joss.01231.

[23] S. van der Walt, S. C. Colbert, and G. Varoquaux, "The NumPy Array: A Structure for Efficient Numerical Computation," *Comp. Sci. Eng.*, vol. 13, no. 2, pp. 22–30, Mar. 2011, doi:10.1109/MCSE.2011.37.

[24] E. Jones, T. Oliphant, and P. Peterson, "SciPy: Open source scientific tools for Python," 2014. [Online]. Available: http://www.scipy.org/

[25] J. D. Hunter, "Matplotlib: A 2D Graphics Environment," *Comp. Sci. Eng.*, vol. 9, no. 3, pp. 90–95, Jun. 2007, doi:10.1109/MCSE.2007.55.

[26] S. K. Lam, A. Pitrou, and S. Seibert, "Numba: a LLVM-based Python JIT compiler," in *Proc. 2nd Workshop LLVM Compiler Infrastructure HPC*, Austin, TX, Nov. 2015, doi:10.1145/2833157.2833162.

[27] J. D. Garrett, B.-K. Tan, C. Chaumont, F. Boussaha, and G. Yassin, *in preparation*.

[28] G. Yassin, R. Padman, S. Withington, K. Jacobs, and S. Wulff, "Broadband 230 GHz finline mixer for astronomical imaging arrays," *Electron. Lett.*, vol. 33, no. 6, pp. 498–500, Mar. 1997, doi:10.1049/el:19970314.

[29] A. Skalare, "Determining embedding circuit parameters from DC measurements on quasiparticle mixers," *Int. J. Infrared Millim. Waves*, vol. 10, no. 11, pp. 1339–1353, Nov. 1989, doi:10.1007/BF01010125.

[30] S. Withington, K. Isaak, S. Kovtonyuk, R. Panhuyzen, and T. Klapwijk, "Direct detection at submillimetre wavelengths using superconducting tunnel junctions," *Infrared Phys. Technol.*, vol. 36, no. 7, pp. 1059–1075, Dec. 1995, doi:10.1016/1350-4495(95)00058-5.

[31] D. C. Mattis and J. Bardeen, "Theory of the Anomalous Skin Effect in Normal and Superconducting Metals," *Phys. Rev.*, vol. 111, no. 2, pp. 412–417, Jul. 1958, doi:10.1103/PhysRev.111.412.

[32] A. R. Kerr, "Saturation by Noise and CW Signals in SIS Mixers," in *Proc. 13th Int. Symp. Space THz Tech.*, Cambridge, MA, Mar. 2002, pp. 11–22.

[33] A. Ermakov, V. Belitsky, P. Y. Aghdam, V. Desmaris, S. Ferm, M. Fredrixon, S. Krause, I. Lapkin, and D. Meledin, "Broken-step Phenomenon in SIS Mixers," in *Proc. 27th Int. Symp. Space THz Tech.*, Nanjing, China, Apr. 2016.

[34] C.-Y. E. Tong, A. Hedden, and R. Blundell, "Gain Expansion and Compression of SIS Mixers," *IEEE Trans. Appl. Supercond.*, vol. 19, no. 3, pp. 309–312, Jun. 2009, doi:10.1109/TASC.2009.2019102.

John Garrett completed a B.Sc. in Electrical Engineering at the University of Alberta in 2012, a M.Sc. in the same field at the University of Calgary in 2014, and a D.Phil. in Astrophysics at the University of Oxford in 2018. His current research is focused on developing wide bandwidth SIS mixers, focal plane arrays, and software for simulating SIS junction behavior. He was the recipient of the ALIS Sir James Lougheed Award of Distinction in 2015, the Clarendon Fund in 2014, and the IEEE Antennas and Propagation Pre-Doctoral Research Award in 2013.

Boon Kok Tan received the B.Eng. degree in Electrical and Electronic Engineering and the M.Eng. degree in Solar Engineering from University of Technology Malaysia, in 2001 and 2003, respectively. He received his D.Phil. degree in Astrophysics from University of Oxford, United Kingdom, in 2012.

Faouzi Boussaha received the engineering diploma in Electronics from the University of Annaba, Annaba, Algeria in 1996 and M.Sc. degree in Electronics, Sensors and Integrated Circuits from the Université de Paris 11 – Orsay, France in 1999 and the Ph.D. degree in astrophysics and space instrumentation jointly from the Université de Paris-6, Paris, and Observatoire de Paris, Paris, France, in 2003. Since 2004, he is with the French National Center for Scientific Research (CNRS) and Observatoire de Paris, Paris, France. In 2010, he was the recipient of a NASA Fellowship and joined the Submillimeter-Wave Advanced Technology Group, Jet Propulsion Laboratory (JPL) NASA, Pasadena, as a NASA Senior Postdoctoral Program Fellow. He also worked on tasks under funding from French Space Agency (CNES). His current research interests at Observatoire de Paris are the design and development of terahertz superconducting devices for radioastronomy.

Christine Chaumont is graduated from UPEC (University of Paris Est-Créteil) in 1987. She has worked in Alcatel-Lucent's research and development laboratories (OPTO+) to develop fast semiconductor laser sources (1.3-1.55 µm) for transmission networks. In 2003, she joined the French National Research Agency (CNRS) within Paris Observatory as part of the GEPI (Galaxies, Stars, Physics and Instrumentation) department. Since then, as an engineer, she is developing superconducting detectors astronomy such as mm/submm and THz SIS (Superconductor-Isolator-Superconductor) as well as near infrared and visible MKIDs (Microwave Kinetic Inductance Detectors).

Ghassan Yassin, photograph and biography not available at the time of publication.